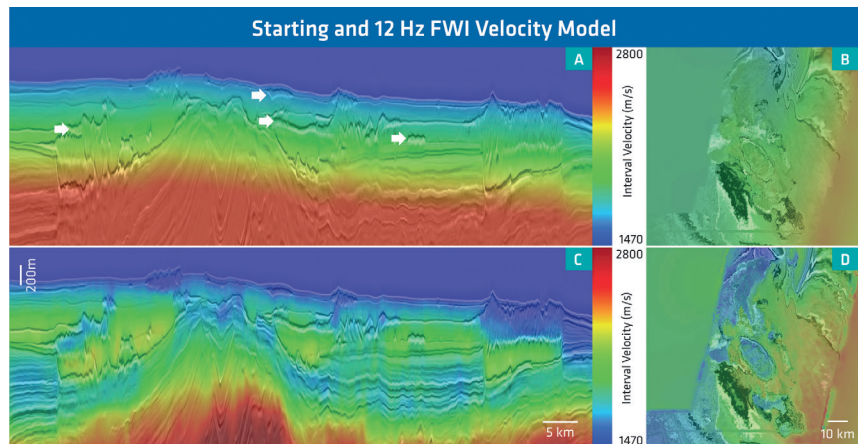


**Figure 2** (A) Beam PSDM stack; (B) an associated shot gather in the full frequency band; and (C) band-limited to 2-4 Hz. Note the complex wavefield below the ooze bodies.



**Figure 3** Beam PSDM stack and 1700 m depth slice with the initial (upper) and final FWI velocity model overlays (lower). A few ooze bodies are labelled with arrows in (A) to highlight their distribution at different depths in the overburden.

emphasizes the long wavelength components of the velocity field, and reduces the reflectivity imprint in the updates. In addition, we built a Q attenuation model that was calibrated with the high-resolution inverted velocity model of the ooze complexes. Small-scale velocity variations and sharp velocity contrasts between the ooze bodies and surrounding lithology were captured with high geological fidelity. From these models we applied a variety of imaging solutions that were able to improve the spatial resolution and quality of the subsurface images.

### FWI theory

Conventional FWI (Tarantola, 1984) solves a nonlinear inverse problem by matching modelled seismic data to recorded field data. The matching is quantified by the residuals of a least-squares misfit function, and the model update is computed as a scaled representation of its gradient. Our modelling engine is based upon an efficient pseudo-analytic extrapolator that ensures the modelling of accurate waveforms free of numerical dispersion (Crawley et al., 2010). The inversion part of our FWI algorithm uses regularized non-linear conjugate gradients to obtain the best-fit velocity model. We used a unique FWI gradient that can utilize both reflected and transmitted waves to produce long wavelength updates (Ramos-Martinez et al., 2016). Thus, the gradient reduces the traditional dominance of high wavenumbers when reflections are involved in the inversion (Brandsberg-Dahl et al., 2017). The fundamental idea is to derive a gradient where the relatively high wavenumber migration isochrones corresponding to specular reflections are removed, and the low wavenumber energy is preserved. This is achieved by inserting dynamic weights into the velocity sensitivity kernel derived from an impedance-velocity parameterization (Ramos-Martinez et al., 2016).

As presented below, our FWI implementation provides reliable velocity updates free of the imprint of reflectivity down to at least 4 km depth when both reflections and refractions are included in the data window for the inversion process.

### Field data example

#### Location

The 3D data presented here from the PGS16004NWS HD3D survey was acquired by PGS MultiClient as the first survey for the new vessel *Ramform Tethys* in 2016, and covers an area of approximately 5500 km<sup>2</sup> in the Outer Vøring area of the Norwegian Sea (refer to Figure 1) encompassing the Nyk High, the Vema Dome, and parts of the Vigrid and Någrind synclines and the Hel Graben. This survey formed part of a much larger 21,000 km<sup>2</sup> dual-sensor multi-client programme acquired by five vessels. Water depth throughout the survey varies between 800-1600 m. Several gas discoveries have been made on the Nyk High, such as Aasta Hansteen (comprising Haklang, Snefrid South, and Luva), Gymir, Roald Rygg and Ivory. The primary reservoir sandstones are the deep marine fans of Cretaceous age such as the Kvitnos, Nise and Springar formations. Neogene-Pleistocene sediments in the overburden include the Naust Formation, which includes many episodes of shelf glaciation, overlying the thick siliceous oozes of the Kai and Brygge formations (Eidvin et al., 1998; Bryn et al., 2005).

Sixteen dual-sensor streamers (GeoStreamers) were towed with 8100 m length (129 km of streamer sections), at that time the largest streamer spread towed in Northern Europe. Pre-survey planning recommended that the streamer separation be reduced to 75 m to optimize shallow data resolution and provide the platform for mitigation of ooze imaging distortion effects. Deep

towing enabled high signal-to-noise ratio (SNR) on both sensors, and useful hydrophone frequencies were recovered down to 2 Hz.

### *FWI workflow and results*

Figure 2 presents a (beam) pre-stack depth migration (PSDM) window with an example shot gather scaled to the same depth window. The 2-4 Hz filtered version of the shot gather highlights the fact that almost no refractions are recorded at any depth for offsets less than about 7 km. Forward modelling of the source wavefield using an iteratively more complex shallow velocity model (increasing the number of layers) also verified that refractions from the base of the ooze cannot be recorded for offsets less than about 6.5 km.

As a result, shallow velocity updates using FWI must mainly rely upon reflected events. The availability of ultra-low frequencies in the dual-sensor data allowed us to start FWI in the 2-4 Hz frequency band with a fairly simple 1D gradient velocity function over the entire survey area without the risk of cycle skipping. Once a sufficient match between the recorded and modelled shots was achieved, the frequencies were gradually increased up to a maximum frequency of 12 Hz. Note that the initial maximum offset modelled was 4 km with a mute function applied to reject

long offset refraction energy. This offset was incrementally increased to 8 km and the mute function was relaxed in the final FWI iterations. Multi-offset hyperbeam reflection tomography was also applied after FWI to optimize residual moveout flatness on image gathers.

Figure 3 shows an overlay of the initial interval velocities and the final FWI velocity model on a representative beam PSDM cross-section and depth slice (1700 m depth). The seismic images clearly show a widespread distribution of complex ooze formations in the area. FWI produced a high-resolution velocity model and managed to capture small-scale velocity variations and sharp spatial velocity contrasts between the ooze bodies and the surrounding lithology. Owing to the aforementioned design features of the FWI kernel, no artifacts or reflectivity imprints are observed in the final FWI velocity model.

### *Refined FWI and imaging results*

Ooze formations tend to have very low interval velocities by comparison to their surrounding lithology; resulting in strong distortion and amplitude dimming effects in the seismic image. Correspondingly, in addition to an accurate velocity model, a detailed Q attenuation model is required in order to produce an optimal image

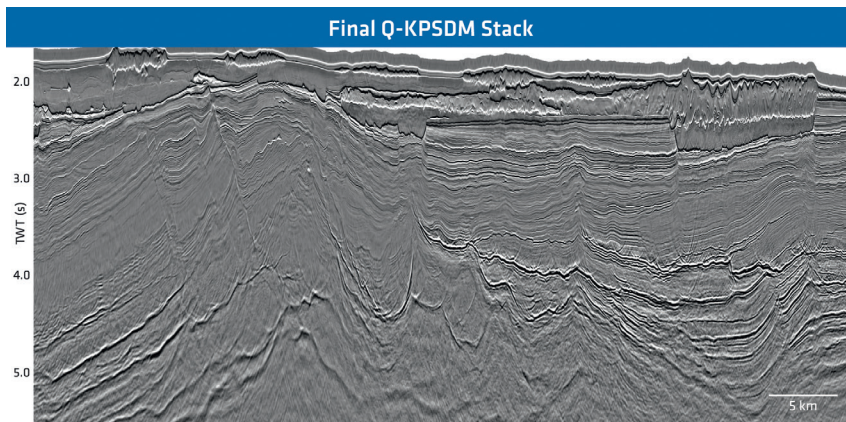


**Figure 4** Final Q-KPSDM full angle GeoStreamer stack revealing large ooze formations with high resolution.

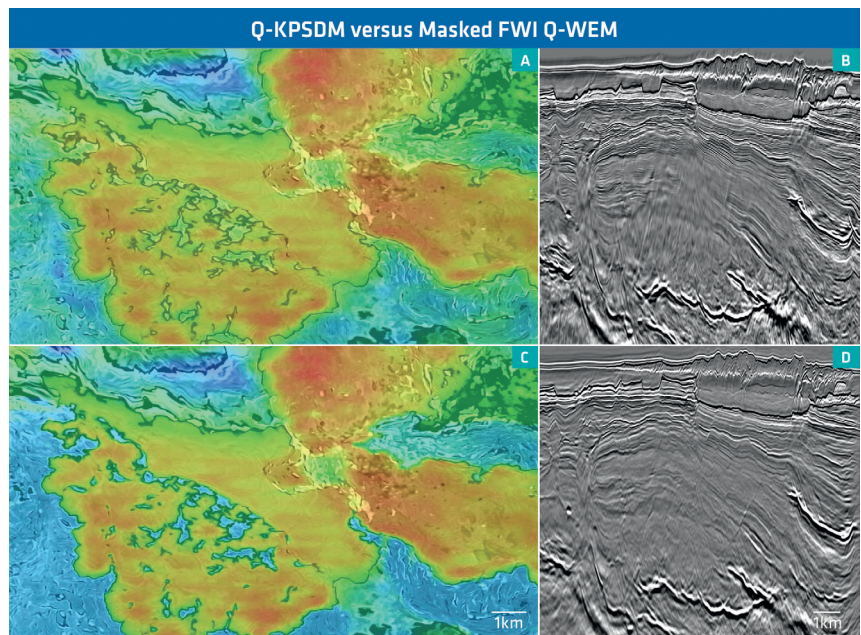


**Figure 5** (A) Q-WEM depth slice (1630 m) with the unmasked FWI velocity model overlay; (B) Q-KPSDM section imaged with the unmasked FWI velocity model; (C) overlay of the masked FWI velocity model used for Q model building; and (D) Q-WEM section imaged with the masked FWI velocity model. Note the improved overall imaging quality in (D) and the superior spatial resolution of faults below the ooze bodies.

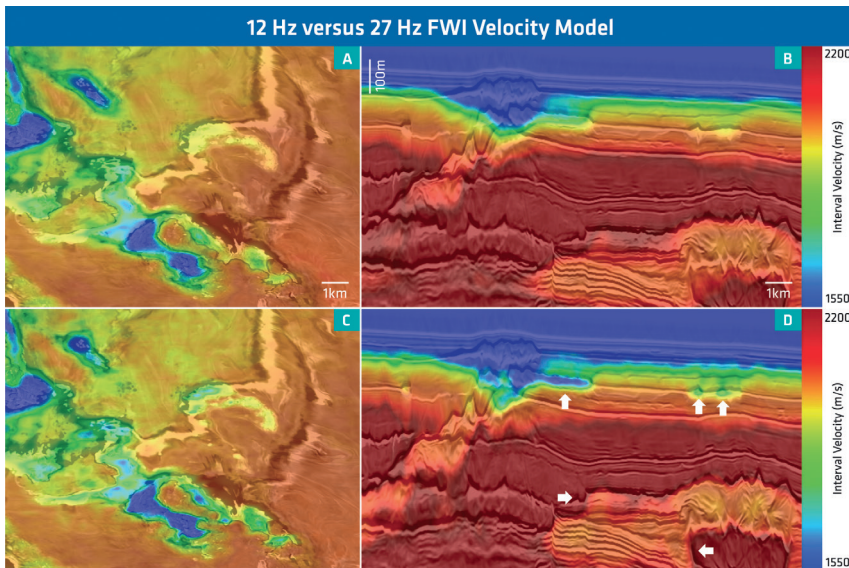


**Figure 6** 12 Hz FWI (upper) and 27 Hz FWI (lower) velocity model overlays on a 1530 m Q-KPSDM depth slice and vertical section. Note the resolution of localized ooze features in the 27 Hz FWI interval velocity model, and the superior spatial delineation of both shallow and deeper ooze bodies. The highlighted feature in the lower right part of (D) is juxtaposed low-velocity shale and ooze.

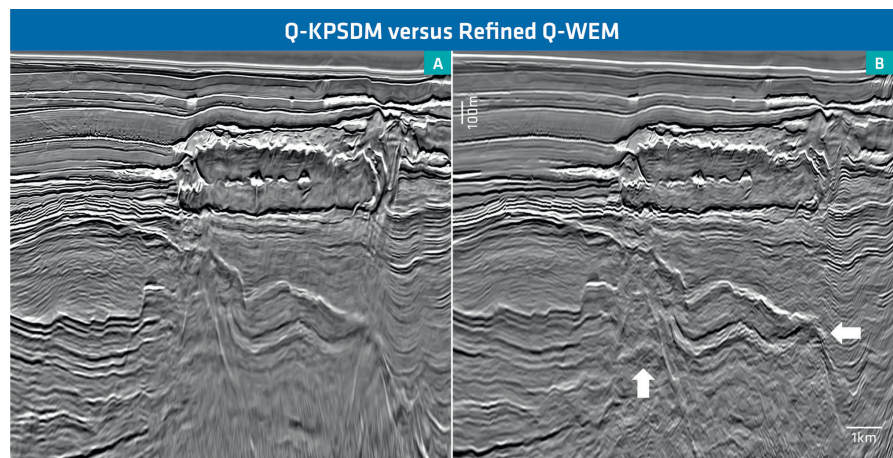


**Figure 7** (A) Q-KPSDM run with the ‘final’ 12 Hz FWI velocity model; and (B) Q-WEM run with the 27 Hz FWI velocity model and masked shallow Q model.

of the subsurface. We used a version of the FWI velocity model to build the production Q model, which assumes that low interval velocities correlate with the less consolidated sediments that cause higher seismic attenuation. Figure 4 shows an example of the final full angle stack imaged with viscoelastic Kirchhoff depth migration (Q-KPSDM). Observe that structures beneath the ooze have been well imaged, while at the same time absorption effects have been successfully compensated within the migration.

A subset of the data volume was also used to test viscoelastic wave equation migration (Q-WEM) run to 60 Hz maximum frequency. A benefit of WEM is that, in contrast to Kirchhoff migration, the input velocity model requires no smoothing, and the migration kernel will better accommodate multi-pathing through local complexities in the velocity model. Furthermore, a masked manual interpretation of the top and base of the ooze bodies was used to insert low Q values into the ooze bodies of the final Q model. Figure 5 illustrates that when the shallow velocity anomalies are accurately resolved without smoothing and when local Q anomalies are included, image distortions throughout the Q-KPSDM result are avoided. When using Q-WEM, general event focusing is cleaner, and the spatial resolution of faults and associated rotated fault blocks is higher.

FWI was also run to 27 Hz on a subset of the data discussed here, resulting in more accurate spatial delineation of the ooze bodies in the interval velocity model (refer to Figure 6). Note how localized ooze bodies below the seafloor are accurately resolved in Figure 6D, and the better definition of low velocity shale juxtaposed against deeper ooze.

Figure 7 compares Q-KPSDM with the unmasked 12 Hz FWI velocity model and original Q model versus Q-WEM with the masked 27 Hz FWI velocity model and the updated Q model. The Q-WEM image is significantly less distorted below the thick ooze body, and as annotated by arrows in Figure 7B, the spatial resolution of faults and various geological contacts and facies boundaries is improved.

Although not pursued here, Feuillebois et al. (2017) demonstrate what high-resolution FWI velocity models can be used to build acoustic impedance models where a ‘low frequency gap’ has historically confronted AVO inversion, generating absolute elastic attributes, and derisking prospects in the absence of local well information. The workflow steps described here, which resolve shallow ooze interval velocity and Q anomalies, will be a necessary component of any such quantitative interpretation workflow.

## Conclusions

We have described a workflow that compensated for the effects of complex oozes upon seismic imaging and amplitude recovery. A gradient-based FWI solution that used both the reflected and refracted wavefields enabled high-resolution velocity updates deeper than the maximum penetration depth of diving waves, free of the imprint of specular reflectivity. The availability of ultra-low frequencies in deep-towed dual-sensor data enabled FWI to begin in the 2-4 Hz frequency band, thereby avoiding cycle-skipping in an area characterized by complex seismic wavefields. A version of the FWI velocity model was used to build the production Q model for Q-KPSDM imaging, and a masked/interpreted velocity model was also used to insert low Q values within the ooze bodies of the final Q model for Q-WEM imaging. Examination of viscoelastic Kirchhoff depth migration (Q-KPSDM) images reveal clear improvements. Resolution of faults and fault block movements around the Gjallar Ridge, the Vema Dome and the Nyk High is demonstrably improved, as is general reflector continuity below the ooze bodies. Additional testing of viscoelastic wave equation migration (Q-WEM) further improved the spatial resolution and quality of seismic images below the ooze bodies, courtesy of being able to use unsmoothed velocity models with local high resolution in zones of complex geology.

## Acknowledgements

The authors would like to thank PGS for permission to publish this work, Statoil for its valuable input during the project, and PGS colleagues Stefan Möller, Martin Wahle, Emma Scala, Omar Baramony, and Andrew Long.

## References

- Brandsberg-Dahl, S., Chemingui, N., Valenciano, A.A., Ramos-Martinez, J. and Qui, L. [2017]. FWI for model updates in large-contrast media. *The Leading Edge*, **36**(1), 81-87.
- Bryn, P., Berg, K., Forsberg, C.F., Solheim, A. and Kvalstad, T.J. [2005]. Explaining the Storegga Slide. *Marine and Petroleum Geology*, **22**, 11-19.
- Crawley, S., Brandsberg-Dahl, S., McClean, J. and Chemingui, N. [2010]. TTI reverse time migration using the pseudo-analytic method. *The Leading Edge*, **29**(11), 1378-1384.
- Eidvin, T., Brekke, H., Riis, F. and Renshaw, D.K. [1998]. Cenozoic stratigraphy of the Norwegian Sea continental shelf, 64°N-68°N. *Norsk Geologisk Tidsskrift*, **78**, 125-151.
- Feuillebois, L.O., Charoing, V., Maioli, A. and Reiser, C. [2017]. Utilizing a novel quantitative interpretation workflow to derisk shallow hydrocarbon prospects — a Barents Sea case study. *First Break*, **35**(3), 85-92.
- Ramos-Martinez, J., Crawley, S., Zou, Z., Valenciano, A.A., Qui, L. and Chemingui, N. [2016]. A robust gradient for long wavelength FWI updates. *78<sup>th</sup> EAGE Conference and Exhibition*, Extended Abstracts, Th SRS2 03.
- Tarantola, A. [1984]. Inversion of seismic reflection data in the acoustic approximation. *Geophysics*, **49**(8), 1259-1266.



## Cloud Services for Subsurface Data at EAGE #1252

Access your seismic, wells and interpretation archives for analysis and data analytics. Katalyst manages the complete subsurface data life cycle for over 18 petabytes of data.

[sales@katalystdm.com](mailto:sales@katalystdm.com)

Visit Katalyst Data Management at EAGE stand 1252.

[katalystdm.com](http://katalystdm.com)

